Molly M. Range, Brian K. Arbic, Brandon C. Johnson, Theodore C. Moore, Alistair J. Adcroft, Joseph K. Ansong, Jeroen Ritsema, and Christopher R. Scotese

The Chicxulub impact produced a powerful global tsunami

Submitted for Publication in:

Nature

in lieu of thesis in partial fulfillment of the requirements for the degree of
Master of Science in Earth and Environmental Sciences
Department of Earth and Environmental Sciences
The University of Michigan
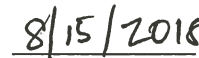Accepted by:

Signature	Name	Date
Theodore D. Moore	Theodore C. Moore, Jr	8/7/2018
Brian K. Arbic	BRIAN K. ARBIC	9/3/2018
Naomi E. Levin (Department Chair Signature)	NAOMI E. LEVIN	8/15/2018

I hereby grant the University of Michigan, its heirs and assigns, the non-exclusive right to reproduce and distribute single copies of my thesis, in whole or in part, in any format. I represent and warrant to the University of Michigan that the thesis is an original work, does not infringe or violate any rights of others, and that I make these grants as the sole owner of the rights to my thesis. I understand that I will not receive royalties for any reproduction of this thesis.

☐ Permission granted.

■ Permission granted to copy after: December 2018

☐ Permission declined.

Molly Range

The Chicxulub impact produced a powerful global tsunami

Molly M. Range[1], Brian K. Arbic[1,2], Brandon C. Johnson[3], Theodore C. Moore[1], Alistair J. Adcroft[4], Joseph K. Ansong[1,5], Jeroen Ritsema[1], and Christopher R. Scotese[6]

[1]Department of Earth and Environmental Sciences, University of Michigan, Ann Arbor, MI, 48109, USA.
[2]Currently on sabbatical at Institut des Géosciences de L'Environnement (IGE), Grenoble, France, and Laboratoire des Etudes en Géophysique et Océanographie Spatiale (LEGOS), Toulouse, France;
[3]Department of Earth, Environmental and Planetary Sciences, Brown University, Providence, RI 02912, USA.
[4]Atmospheric and Oceanic Sciences Program, Princeton University, Princeton, NJ 08540, USA.
[5]Department of Mathematics, University of Ghana, Legon Boundary, Accra, Ghana.
[6]Department of Earth and Environmental Sciences, University of Texas, Arlington, TX, 76109, USA.

An approximately 14-km diameter asteroid is implicated in the Cretaceous/Paleogene (K/Pg) mass extinction[1]. The bolide impact caused global temperature fluctuations[1], large aerosol[2], soot and dust plumes[3], and wildfires from ejecta re-entering the atmosphere[4,5]. Drilling cores from the International Continental Drilling Program (ICDP) and the Integrated Ocean Drilling Program[6] (IODP) revealed the exact physical and geophysical nature of the crater and its peak ring and facilitated the modeling of the impact event[7]. There have been regional tsunami simulations of the impact region of the Chicxulub impact within the Gulf of Mexico by Ward[8] and Matsui et al.[9] Here we present the first global simulation of the Chicxulub impact tsunami from initial contact of the projectile to global propagation using a hydrocode to model the displacement of water, sediment, and crust over the first ten minutes, and a shallow-water ocean model from that point onwards. The tsunami due to the impact and subsequent submarine landslides on the marine shelf[10] was approximately 2700 times more energetic than the December 26, 2004 Indian Ocean tsunami, one of the largest tsunamis in the modern record. Flow velocities exceeded 20 cm/s along shorelines worldwide and disturbed sediments over 6000 km from the impact origin.

Most global tsunami simulations to date have been of tsunamis induced by underwater earthquakes, for instance, the 2004 Indian Ocean tsunami[11]. Such tsunamis have traditionally been simulated with shallow-water ocean models, which assume static bathymetry and hydrostatic conditions. They cannot be used to simulate the complex first ten minutes or so of the K/Pg impact tsunami when there was large-scale deformation of the crust, crater formation[7], and the creation of a collapse wave after water fills the crater. This secondary collapse wave produces much of the energy and propagation of the tsunami that followed the impact. The collapse wave and post-impact, ejecta splashing back into the ocean create highly non-hydrostatic waves. Modeling the impact and immediate post-impact conditions requires an evolutionary model of the crater formation, and of non-hydrostatic water waves.

We use the axisymmetric iSALE-2D hydrocode[12,13] to simulate the initial formation of the Chicxulub impact tsunami for the first time. We assume radial symmetry of the iSALE hydrocode results at ten minutes post-impact, and merge them into a shallow-water model [the Geophysical Fluid Dynamics Laboratory (GFDL) Modular Ocean Model Version 6[14], MOM6] to trace the tsunami through the world ocean. The results of our impact simulation for a 1-km thick ocean are shown in Fig 1. About 2.5 minutes after contact of the projectile, a curtain of ejecta

has produced a 4.5-km-high wave in front of it (Fig. 1a). After 5 minutes, ejecta are emplaced as discontinuous clumps and still imparting momentum to the ocean (Fig. 1b). At 10 minutes, when ejecta are no longer being emplaced, a 1.5-km-high tsunami at 220 km from the point of impact begins to propagate through the deep ocean. The crater and water wave structure at these early times do not depend strongly on assumed ocean depth. The dimension and formation of the crater are similar to previous work[7,15].
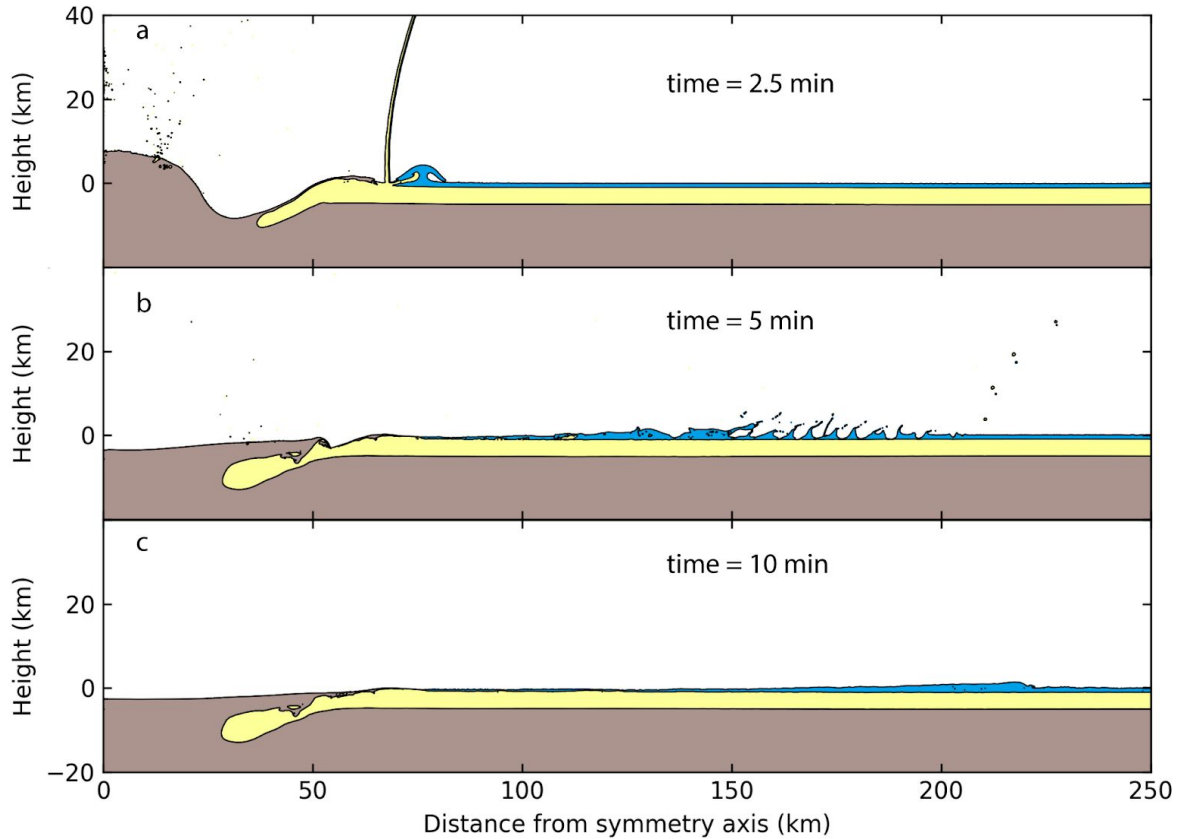

Figure 1: Formation of Chicxulub crater and the associated tsunami. Time series with material colored according to material type (crustal material is brown, sediments are yellow, and the ocean is blue). The origin marks the point of impact. Black curves mark material interfaces (e.g., sediment-crust interface).

The axisymmetric nature of our high-resolution hydrocode model requires that the ocean layer has a constant thickness. Estimates of paleobathymetry show that water depth ~1km where ejecta emplacement produces the initial rim-wave (50-km from basin center). At ~150-km from the point of impact the ocean is ~3 km deep (Fig 2). To test for sensitivity to pre-impact ocean depth we vary the thickness of the ocean layer from 1–3 km (waveforms shown in Extended Data A). Our two-dimensional axisymmetric model with a constant depth is clearly a simplification of the asymmetrical bathymetry in the Gulf of Mexico. Moreover, the unprecedented resolution of our hydrocode simulation of 100m is similar to the ocean depth of 100-200m at the impact site. An ocean depth greater than 100-200m is needed to obtain realistic results with the hydrocode. Two initial conditions were created based on the 1-km ocean depth

hydrocode results. A sediment rim on the impact crater ten minutes into the run came above the water column, creating an annulus shaped island. When this sediment rim is placed on the Gulf of Mexico bathymetry, the sediment rim is entirely underwater. As the rim is composed of loose sediment, it would have been quickly dispersed by wave action[16]; however, we model one initial condition with this sediment rim and one without. We tested for sensitivity between the two runs and found the energies comparable (not shown). The 1-km water depth with no sediment rim is used for all runs.

For the open-ocean simulation, MOM6 is run as a shallow-water model assuming hydrostatic conditions, with wetting and drying, ideal for modeling tsunami propagation. To accurately simulate tsunami propagation, a paleobathymetry was combined with the initial condition from the hydrocode results. We merged two paleobathymetry datasets. The Müller et al. dataset[17] uses basin age-depth relationship for 66 Ma bathymetry. The PALEOMAP database of Scotese[18] is reconstructed from present-day crust back to 66 Ma. Destroyed continental crust was not reconstructed. Since most of the old ocean crust has been subducted, there is only a partial bathymetry where Scotese could reposition plates that are still present today. Where the two paleo-geographies do not match in depth, data from PALEOMAP was given more weight along coastlines, continental margins, and the Gulf of Mexico. For deep-water and ocean basins, Müller et al. was given a larger weight. Along the west coast of North America and the east coast of Asia where older crust has been subducted, there are regions that Müller et al. considered to be land, and Scotese had considered to be water at uniform depth of 5000m. A constant intermediate depth of 4200m was assigned to these locations. After combining the two datasets, the bathymetry was smoothed and water shallower than 1m was assigned as land.

Motivated by impact simulations that reproduce the seismically observed structure of Chicxulub[14] as well as the peak shock pressures and composition of the basin's peak-ring, as constrained by recent drilling[7], we assume the 14-km-diameter impactor has a density of 2650 kg/m^3 and strikes Chicxulub at 12 km/s. We model the target as a granitic crust overlain by a 4-km-thick layer of sediments and an ocean.
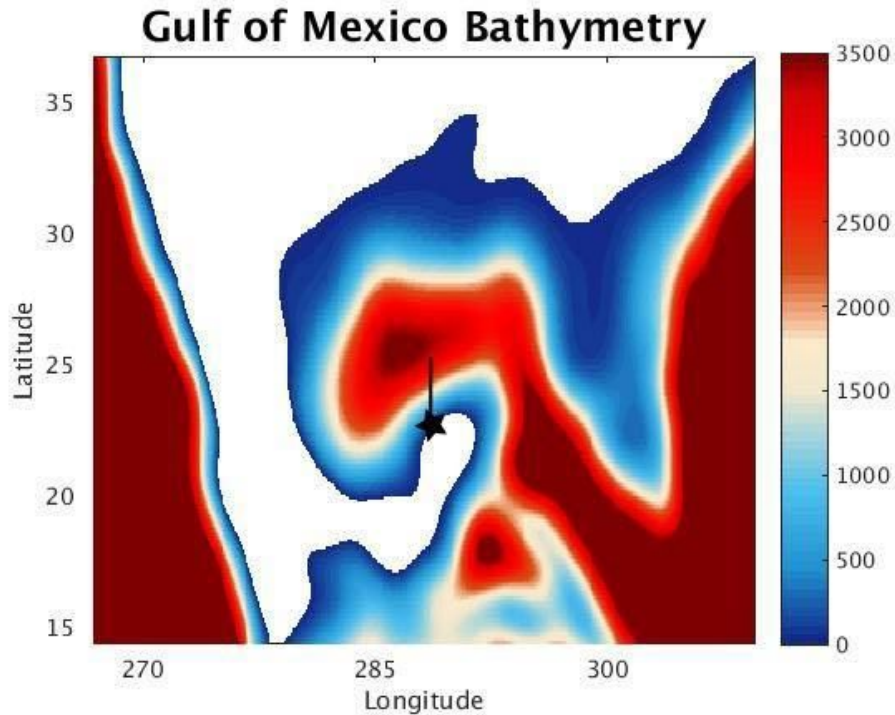
Figure 2: Pre-impact K/Pg bathymetry of Gulf of Mexico in meters. The impact occurred in shallow water of 100-200m, at the location indicated by a star. At >50 km from the impact, the Gulf of Mexico is deeper than 1000 m, the depth used in the hydrocode simulation shown in Fig. 1. The black line shown above has a length of 250-km, the length of the domain used in the hydrocode simulation.

A conversion from the axisymmetric, constant water depth conditions assumed by the hydrocode to more realistic, non-axisymmetric conditions, with a water depth that varies in both horizontal directions, was necessary to continue the simulation with the MOM6 code. The hydrocode results at 600 seconds post-impact are used for the MOM6 initial condition; at this time there are no more falling ejecta in the region and there is a defined waveform in approximate hydrostatic balance. The waveform, crater shape and velocity are isolated from the density profile and, by assuming radial symmetry, converted into a ring-shaped wave dependent on resting sea level. For more information, see Extended Data B.

The MOM6 flow velocity and sea surface height were output every hour over ten days. Fig 3. displays the perturbation sea surface height of the progressing tsunami over time. The impact tsunami spread quickly into the Atlantic (Fig. 3b,c) and through the Central American seaway into the Pacific (Fig. 3d), where its propagation can be traced for at least 24 hours post-impact (Fig. 3e). The tsunami front propagates in excess of 200 m/s in deep water. By 48 hours post-impact, the tsunami amplitude pattern is complex due to wave reflection and refraction (Fig 3f). These (open-ocean) sea surface height anomalies rarely exceed ±1m; however, when a tsunami reaches the shallow waters of a coastline, the wave amplitude increases due to shoaling. Depending on the exact geometries of the coast and the advancing waves, some coastal regions could be inundated and eroded. The models used here do not estimate wave run-up onto land[9],

nor is our knowledge of global coastal bathymetry and topography at 66 Ma adequate to make predictions of coastal flooding and erosion.
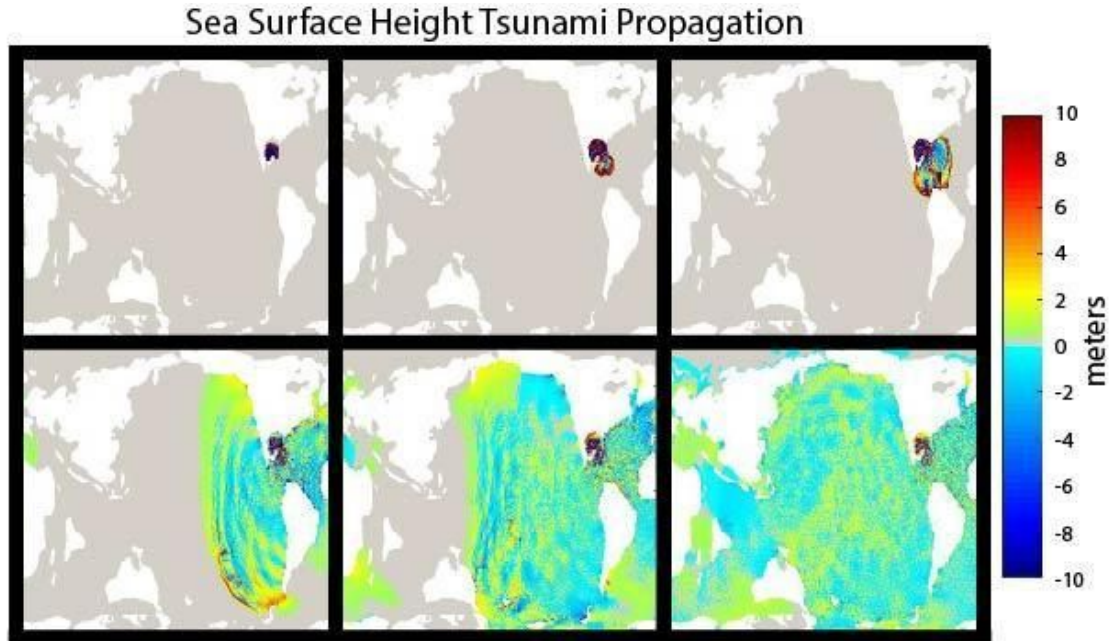

Figure 3: Sea surface height in meters at A) 1 hour, B) 3 hours, C) 5 hours, D) 16 hours, E) 24 hours, and F) 48 hours post impact.

The maximum velocity at each model grid cell over the ten-day simulated time is shown in Fig 4. Near the impact, the flow velocity exceeds 30 m/s in the initial wave. Flow velocities can be a factor of 100 times smaller in the middle of the ocean than it is near the impact origin and along the coasts. Flow velocities lower than 20 cm/s are not shown because they are not expected to cause erosion of fine grained pelagic sediments[19]. Velocities higher than 20 cm/s are predicted in the North Atlantic and the equatorial region of the South Atlantic, in the Central American seaway and in most of the southern and southeastern Pacific, more than 12,000 km from the impact area. Tsunami propagation and flow velocities of prior simulations are shown in Extended Data C.
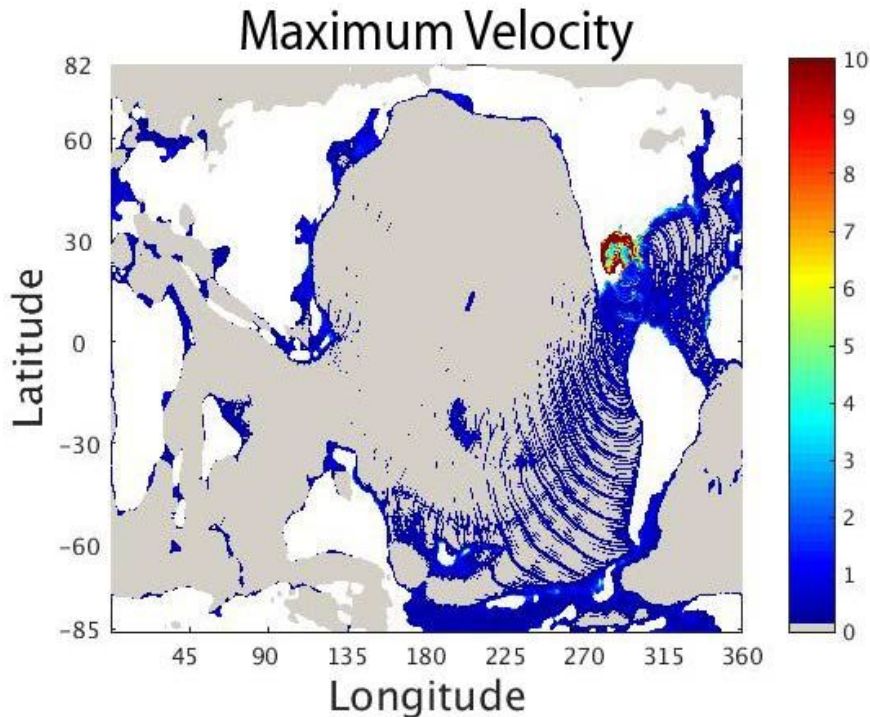
Figure 4: Maximum Velocity at each grid cell where all points where flow velocity is under 20 cm/s are greyed out. Extended Data D shows a closer view of the Gulf of Mexico

Open-ocean areas in the Tethyian region, the South Atlantic, the North Pacific, and the Indian Ocean appear geographically protected from the tsunami. Flow velocities exceed 20 cm/s in shallow-marine areas, over bathymetric highs, and along coastlines worldwide. Whether or not the impact tsunami caused near shore and shallow-water erosion in a particular area depends on the exact nature of the coastal configurations, coastal topography, and the surrounding bathymetry. These details are beyond our ability to resolve with this model. However, where these disturbances are preserved in the marine sedimentary deposits, we can perhaps estimate flow velocities from the sediment record and compare these estimates to the modeled flow velocities. Our tsunami model suggests that the bolide impact not only had major effects on the global atmosphere and biosphere, it also created a tsunami of such magnitude that its effect is felt across much of the world ocean. To give a perspective on how large the impact tsunami was, we compare, in Extended Data E, the total energy of the impact tsunami with the energy of the 2004 Indian Ocean tsunami[11]. The impact tsunami is found to be have an energy about 2700 times larger.

In future work we will examine K/Pg stratigraphic sections from marine deposits studied on land and in drill cores from the deep-sea that recovered a K/Pg boundary section. At the very least these records should indicate if the global distribution of flow velocities of the Chicxulub tsunami is consistent with records of well-preserved and eroded uppermost Cretaceous sediments, including reworked older sediments, rip-up clasts, erosional truncation of sedimentary

features, and missing biostratigraphic zones and coarser grained deposits in the uppermost Cretaceous interval. In their survey of deep sea drill sites MacLeod and Keller[20] state that "…virtually all deep-sea boundary sequences are
marked by intervals of non-deposition or hiatus formation during the latest Cretaceous…" Yet we are hopeful that where the K/Pg boundary is preserved, the records will indicate if the pathways of the tsunami model is consistent with records of well preserved versus eroded uppermost Cretaceous sediments.

Author Contributions: MMR converted the hydrocode results into the initial conditions for the MOM6 tsunami simulations, ran the MOM6 simulations, and wrote the paper. BKA implemented and oversaw the project. BCJ ran the iSALE hydrocode simulations and greatly contributed to the design of the final simulations. TCM conceived the project in a conversation with BKA and contributed geologic interpretation. AJA and JKA set up the MOM6 model on University of Michigan computers. JKA also helped MMR to run the MOM6 models and construct initial conditions. JR helped to refine the initial conditions. CRS provided the bathymetry for the K/Pg Boundary. All authors contributed to improving the manuscript.

References
1. Schulte, P. *et al.* The Chicxulub asteroid impact and mass extinction at the Cretaceous-Paleogene boundary. *Science* **327,** 1214–8 (2010).
2. Bardeen, C. G., Garcia, R. R., Toon, O. B. & Conley, A. J. On transient climate change at the Cretaceous-Paleogene boundary due to atmospheric soot injections. *Proc. Natl. Acad. Sci. U. S. A.* **114,** E7415–E7424 (2017).
3. Brugger, J., Feulner, G. & Petri, S. Baby, it's cold outside: Climate model simulations of the effects of the asteroid impact at the end of the Cretaceous. *Geophys. Res. Lett.* **44,** 419–427 (2017).

4.   Morgan, J., Artemieva, N. & Goldin, T. Revisiting wildfires at the K-Pg boundary. *J. Geophys. Res. Biogeosciences* **118,** 1508–1520 (2013).

5.   Busby, C. J., Yip, G., Blikra, L. & Renne, P. Coastal landsliding and catastrophic sedimentation triggered by Cretaceous-Tertiary bolide impact: A Pacific margin example? *Geology* **30,** 687–690 (2002).

6.   Morgan, J. *et al.* IODP 548-Full3 CHICXULUB: DRILLING THE K-T IMPACT CRATER Contact Proponents Co-Proponents.

7.   Morgan, J. V. *et al.* The formation of peak rings in large impact craters. *Science* **354,** 878–882 (2016).

8.   Ward, S. *https://www.youtube.com/watch?v=Dcp0JhwNgmE*. (2012); Matsui, T, F. Imamura, E. Tajika, Y. Nakano, and Y. Fujisawa, 2002. Generation and propagation of a tsunami from the Cretaceous-Tertiary impact event. in Koeberl, C., and MacLeod, K.G., eds., Catastrophic Events and Mass Extinction: Impacts and Beyond: Geological Society of America Special Paper 356, p. 55–69.

9.   Matsui, T., Imamura, F., Tajika, E., Nakano, Y. & Fujisawa, Y. Generation and propagation of a tsunami from the Cretaceous-Tertiary impact event propagation of a tsunami from the Cretaceous-Tertiary impact event, in. (2002).11.

10.   Gulick, S. P. S. *et al.* Importance of pre-impact crustal structure for the asymmetry of the Chicxulub impact crater. (2008). doi:10.1038/ngeo103

11.   Adcroft, A. NOAA-GFDL/MOM6-examples. *GitHub* (2017). at https://github.com/NOAA-GFDL/MOM6-examples/wiki

12.   Collins, G. S., Melosh, H. J. & Ivanov, B. A. Modeling damage and deformation in impact simulations. *Meteoritics & Planetary Science* **39,** 217–231 (2004).

13.   Wünnemann, K., Collins, G. S. & Melosh, H. J. A strain-based porosity model for use in hydrocode simulations of impacts and implications for transient crater growth in porous targets. *Icarus* **180,** 514–527 (2006).

14.   Collins, G. S. *et al.* Dynamic modeling suggests terrace zone asymmetry in the Chicxulub crater is caused by target heterogeneity. *Earth Planet. Sci. Lett.* **270,** 221–230 (2008).

15.   Bell, C., Morgan, J. V, Hampson, G. J. & Trudgill, B. Stratigraphic and sedimentological observations from seismic data across the Chicxulub impact basin. *Meteorit. Planet. Sci.* **39,** 1089–1098 (2004).

16.   Müller, R. D., Sdrolias, M., Gaina, C. & Roest, W. R. Age, spreading rates, and spreading asymmetry of the world's ocean crust. *Geochemistry, Geophys. Geosystems* **9,** (2008).

17.   Scotese, C. R. *The PALEOMAP Project: paleogeographic atlas and plate tectonic software. The PALEOMAP Project: paleogeographic atlas and plate tectonic software* (1997).

18.   McCave, I. N. Erosion, transport and deposition of fine-grained marine sediments. *Fine-grained sediments; Deep. Process. facies* **15,** 35–69 (1984).

19.   Smith, W., Scharroo, R., Titov, V., Arcas, D. & Arbic, B. Satellite Altimeters Measure Tsunami—Early Model Estimates Confirmed. *Oceanography* **18,** 11–13 (2005).

20.   MacLeod, K.G. & Keller, G. Hiatus distributions and mass extinctions at the Cretaceous/Tertiary boundary. *Geology* **19**, 497-501 (1991).

Extended Data

Waveform from Hydrocode of 1000m, 2000m, 3000m
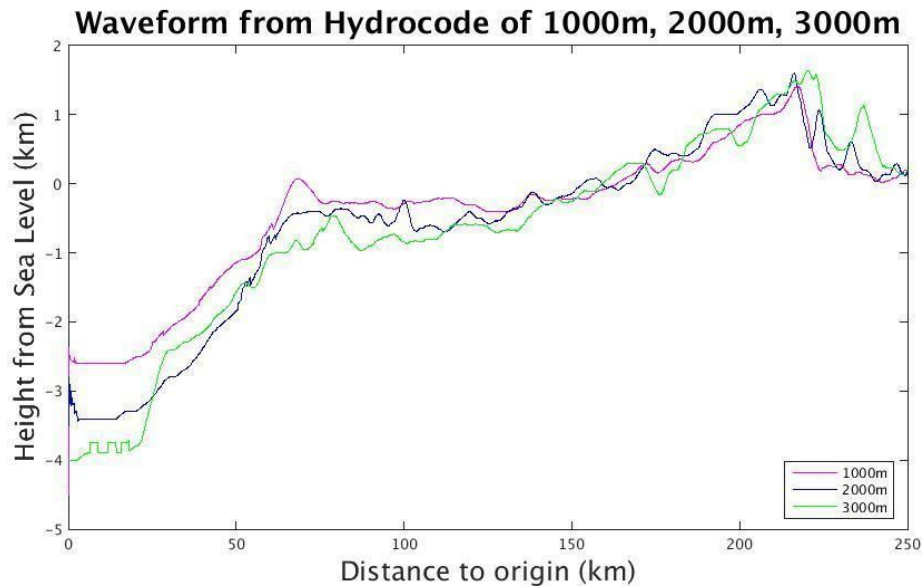
Extended Data A: Waveform for three different runs from hydrocode. The crater lines are displaced by 1 km each because of the differing ocean depths from the run.

Extended Data B: Initial Conditions

In the hydrocode results, each grid cell in the density profile has a specific velocity for the matter that is in the cell: air, water, sediment, crystalline basement, or a mixture of one or more of these. The water-filled density cells are isolated, as well as the cells that contain the crater, and a waveform that is centered at resting sea level is created. This waveform is converted from an axisymmetric plot into a ring-shaped wave. The sediment rim is removed and the bathymetry is set as average resting sea level. It is then interpolated to a 1/10th degree resolution and smoothed. This wave and crater region is then placed on top of the initial seafloor topography by adding or subtracting water according to the hydrocode output as specified below in greater detail. To create the velocities for the initial condition, the density profile is used to isolate the water-filled cells and average the water column velocity. The average velocity line is converted into a ring shape, using the same method as the sea surface initial condition. The velocity was then split into zonal and meridional velocity vectors to be put into the model.

Initial Seafloor Topography

Because the hydrocode simulation covers points within 250 km of the impact origin, all such points will be part of the initial condition for the shallow-water model, set by the outputs of the hydrocode. Let the coordinates of a target point, within 250 km of the impact origin, be (x,y). Let $H_{before(x,y)}$ be the topography of the target point before impact (defined by the merging of the Scotese and Müller datasets, described earlier). The sign of H_{before} informs us about whether the target point was land (negative H_{before} value) or ocean (positive H_{before} value) prior to impact.

Outputs of Hydrocode

The hydrocode outputs two quantities that will be used as an initial condition for our shallow-water model; sea surface elevation perturbations, and perturbations to the seafloor depth. Because we assume radial symmetry, we write the output of the hydrocode in terms of a radial distance from the impact point to a target point of interest. Let the distance from our target point to the impact origin be r.

$eta_{hydrocode(r)}$ is the perturbation to sea level given by the hydrocode, in columns where water exists. Of course, in columns near the impact, there is no water at the end of the hydrocode simulation (600 seconds after impact).

Let $H_{hydrocode(r)}$ be the vertical distance between the seafloor prior to impact and the seafloor at the end of the hydrocode simulation. Again, we take positive values of $H_{hydrocode}$ to denote a deepening of the seafloor. We note that seafloor can be either sediment or crystalline basement.

Blending of Hydrocode Results and Initial Seafloor Topography

If $H_{before(x,y)} + H_{hydrocode(r)} > 0$, then we declare the point (x,y) as being water. Negative values of this sum imply that the target point is land.

For the post-impact points that are water, the new bathymetry (seafloor depth below resting sea level) is $H_{before(x,y)} + H_{hydrocode(r)} + eta_{hydrocode(r)}$.

Extended Data C: Various Initial Conditions

Extended Data C1 shows the tsunami propagation through the world ocean for the simulation ('Half Crater') where the crater is only on grid cells that were originally water before impact. Extended Data C2 and C3 show the maximum velocity for this run. Extended Data C4 shows the tsunami propagation for the world ocean for the simulation ('Crater Only') where the crater is a full 360 degrees on land points and water points, but there is no wave added with the crater. This shows that the secondary collapse wave still creates a large wave that travels throughout the ocean, without having the rim wave from the contact of the projectile. Extended Data C5 and C6 show the maximum velocity for this run.
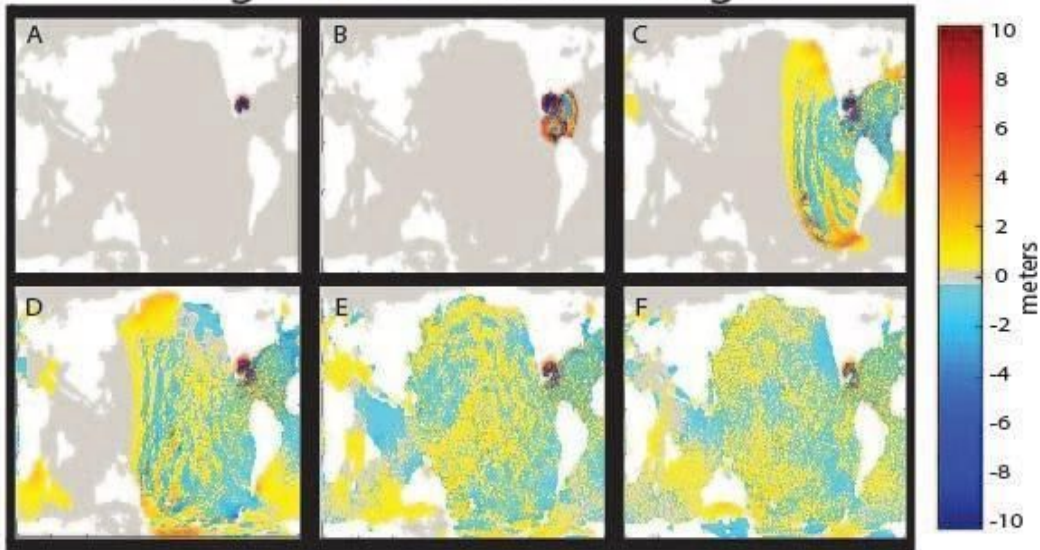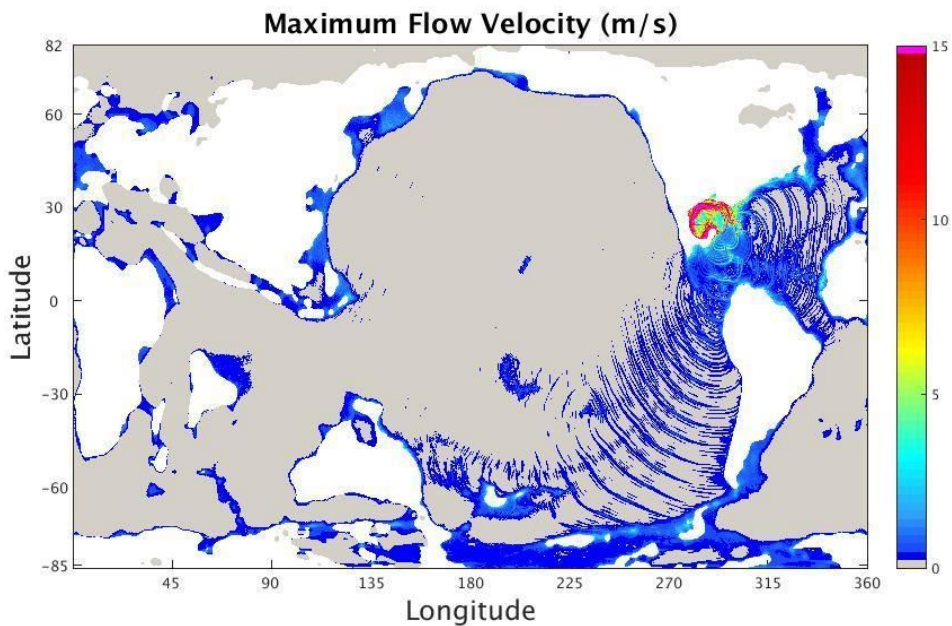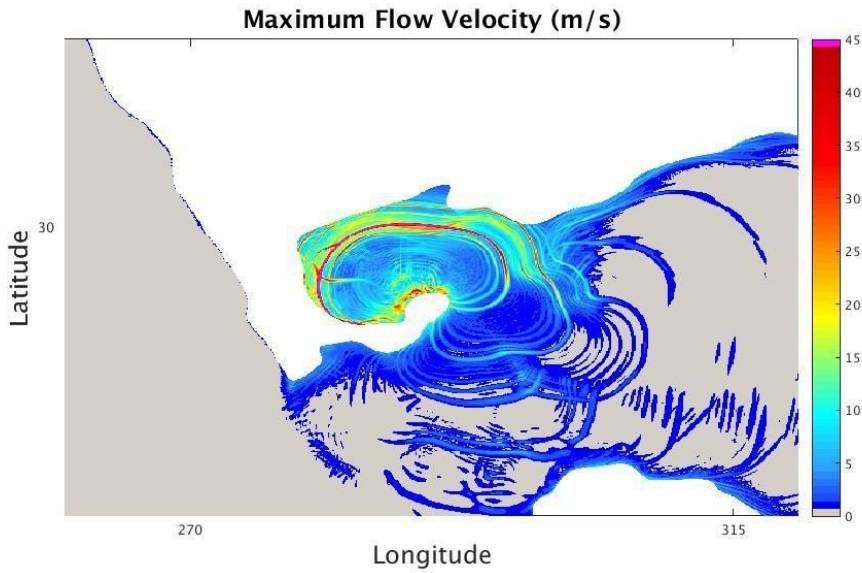
Figure C1: Sea surface height in meters at A) 1 hour, B) 5 hours, C) 16 hours, D) 24 hours, E) 48 hours, and F) 72 hours post impact.
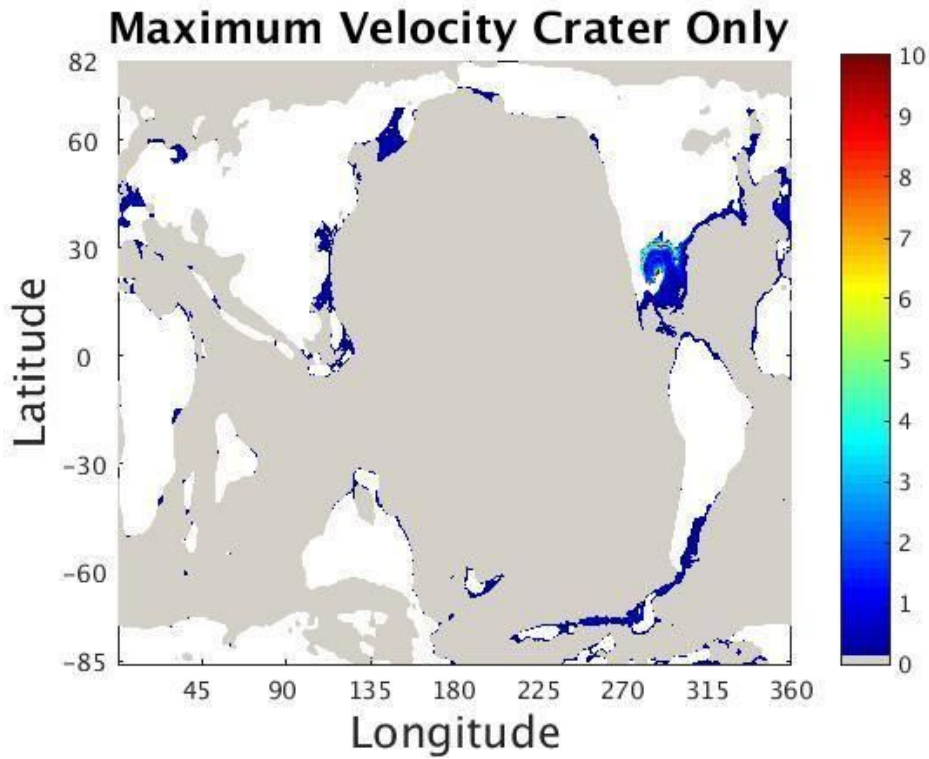

Extended Data C2: Maximum Velocity at each grid cell where all points where flow velocity is under 20 cm/s are greyed out.
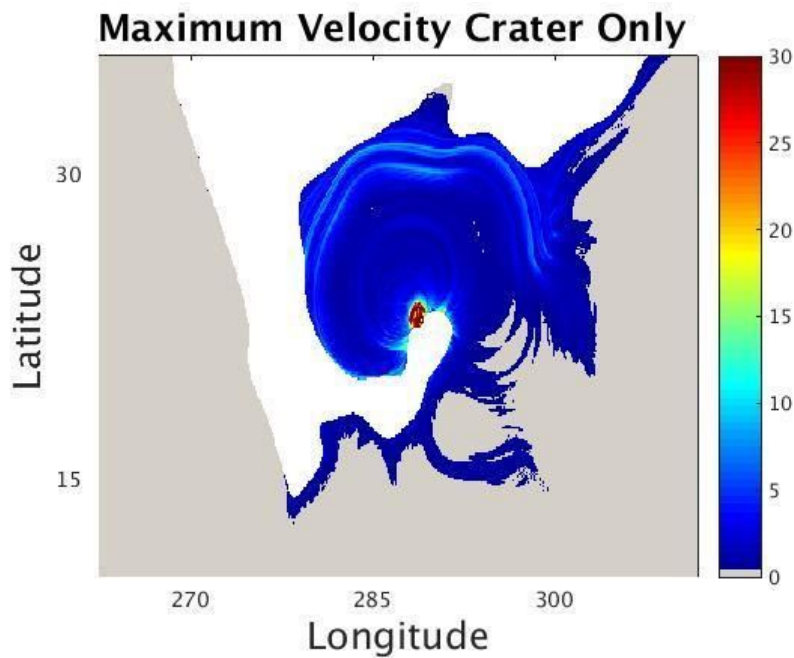
Maximum Flow Velocity (m/s)

Extended Data C3: Maximum Velocity at each grid cell where all points where flow velocity is under 20 cm/s are greyed out.



Sea Surface Height Tsunami Propagation
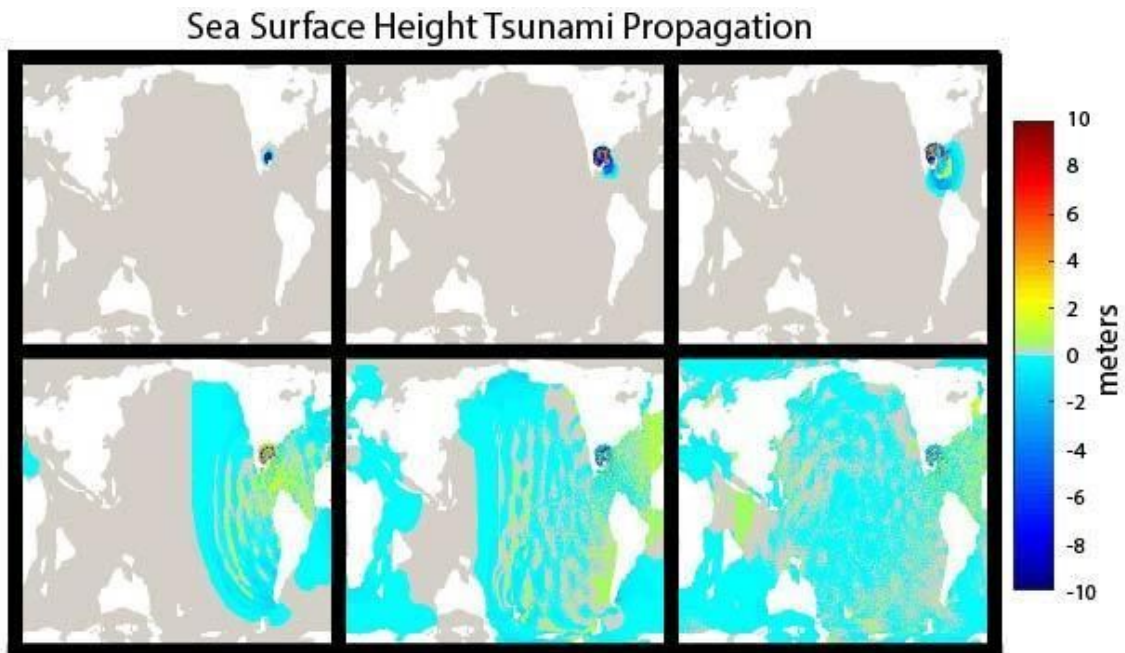
Extended Data C4: Propagation of crater only tsunami. Values are predominantly negative because of the collapse wave filling into the crater.

Extended Data C5: Maximum Velocity at each grid cell where all points where flow velocity is under 20 cm/s are greyed out.

Extended Data C6: Maximum Velocity at each grid cell where all points where flow velocity is under 20 cm/s are greyed out.

Maximum Velocity Full Crater
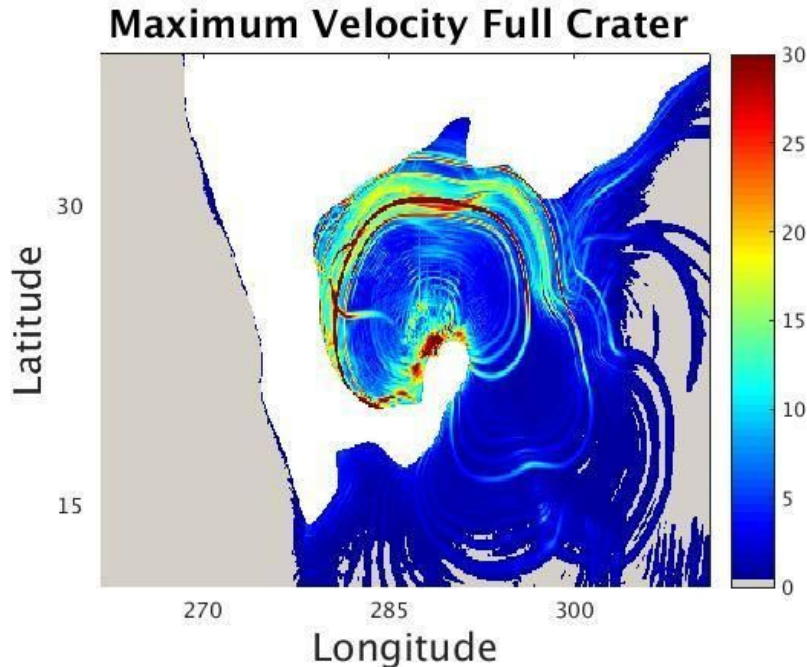
Extended Data D: Maximum Velocity at each grid cell where all points where flow velocity is under 20 cm/s are greyed out.

Extended Data E: Energy

The Indian Ocean Tsunami was triggered by a submarine earthquake and consequent seafloor displacement. This modern-day earthquake-generated tsunami caused large-scale destruction to a number of countries on the Indian Ocean coastline. We chose energy values four hours after the initial condition, in order to allow shocks to damp out of the system. Compared to the Indian Ocean tsunami, the total energy of the impact tsunami appears to be about 2700 times larger. A tsunami of this magnitude has not been seen in recorded history. We tested having a crater purely in water ('Half Crater'), as well as a more complete crater that extended onto land ('Full Crater'). To verify that the collapse wave is the primary source of energy in the wave, we ran a simulation ('Crater Only') where there was no rim wave or velocity, with only a crater for the water to come back in. Energy levels between the half and full crater are comparable. The crater only simulation still has more energy than the Indian Ocean Tsunami.

Table E1	Total Energy (J)
Half Crater Tsunami	$3.7 * 10^{19}$
Indian Ocean Tsunami	$1.4 * 10^{16}$
Full Crater	$3.9 * 10^{19}$
Crater Only	$3.0 * 10^{18}$

Extended Data Table E1: Energy values four hours post impact compared to the 2004 Indian Ocean Earthquake and Tsunami, and various tsunami runs. Energy values were calculated from the model input.